HHS Public Access

Author manuscript

J Immunol. Author manuscript; available in PMC 2020 December 01.

Published in final edited form as:

J Immunol. 2019 December 01; 203(11): 2899–2908. doi:10.4049/jimmunol.1900395.

Folliculin Interacting Protein-1 Maintains Metabolic Homeostasis During B Cell Development by Modulating AMPK, mTORC1, and TFE3

Julita A. Ramírez[*,†], **Terri Iwata**[*], **Heon Park**[*], **Mark Tsang**[*,Ψ], **Janella Kang**[*], **Katy Cui**[*], **Winnie Kwong**[*], **Richard G. James**[π], **Masaya Baba**[§,♯], **Laura S. Schmidt**[§,¶], **Brian M. Iritani**[*,‡]

[*]The Department of Comparative Medicine, University of Washington, Seattle, Washington, USA

[§]Urologic Oncology Branch, Center for Cancer Research, National Cancer Institute, National Institutes of Health, Bethesda MD, USA

[¶]Basic Sciences Program, Frederick National Laboratory for Cancer Research, Frederick MD 21702, USA

[π]Seattle Children's Research Institute, Seattle Washington, USA

Abstract

Folliculin Interacting Protein-1 (Fnip1) is a cytoplasmic protein originally discovered through its interaction with the master metabolic sensor 5' AMP-activated protein kinase (AMPK) and Folliculin (FLCN), a protein mutated in individuals with Birt-Hogg-Dubé Syndrome. In response to low energy, AMPK stimulates catabolic pathways such as autophagy to enhance energy production, while inhibiting anabolic pathways regulated by mechanistic target of rapamycin complex 1 (mTORC1). We previously found that constitutive disruption of *Fnip1* in mice resulted in a lack of peripheral B cells due to a block in B cell development at the pre-B cell stage. Both AMPK and mTORC1 were activated in *Fnip1*-deficient B cell progenitors. In this study we found inappropriate mTOR localization at the lysosome under nutrient-depleted conditions. *Ex vivo* lysine or arginine depletion resulted in increased apoptosis. Genetic inhibition of AMPK, inhibition of mTORC1, or restoration of cell viability with a Bcl-x_L transgene failed to rescue B cell development in *Fnip1*-deficient mice. *Fnip1*-deficient B cell progenitors exhibited increased nuclear localization of Transcription Factor Binding to IgHM Enhancer 3 (TFE3) in developing B cells, which correlated with increased expression of TFE3-target genes, increased lysosome numbers and function, and increased autophagic flux. These results indicate that Fnip1 modulates autophagy and energy response pathways in part through regulation of AMPK, mTORC1, and TFE3 in B cell progenitors.

[‡]**Corresponding Author**: Brian M Iritani, Department of Comparative Medicine, University of Washington, I-438 Health Sciences Center, 1959 NE Pacific St., Seattle WA 98195-7340 USA, Phone: (206) 221-3932, Fax: (206) 685-3006, biritani@uw.edu.
[♯]International Research Center for Medical Sciences (IRCMS), Kumamoto, Japan
[†]Taconic Biosciences, Germantown NY, USA
[Ψ]Gilead Sciences, Seattle, WA, USA

Disclosures

The authors declare no financial conflicts of interest.

Introduction

Developing B cells must pass through well-defined checkpoints, which ensure they are capable of producing functional Ab molecules with minimal self-reactivity. Emerging evidence suggests that B cells may also be regulated by metabolic checkpoints which ensure that mature B cells are appropriately equipped with the molecular machinery to fuel cellular growth required for clonal expansion and Ab production. For example, B cell-specific disruption of *Raptor*, a positive regulator of mTORC1, inhibits pre-B cell metabolism and triggers a complete block in B cell development at the pre-B cell stage, suggesting pre-BCR-driven cell growth may act as a checkpoint for testing metabolic capacity(1). Similarly, mice deficient in PI3K and PLCγ1/PLCγ2, positive mediators of mTOR signaling, also exhibit blocks in B cell development at the pre-B cell stage(2-5). Conditional deletion of *Raptor* during peripheral B cell development inhibits the generation of plasma cells and germinal center B cells (see (6) for review), suggesting that metabolic checkpoints might also regulate peripheral B cell maturation.

Despite abundant information about the roles of mTORC1 in the development of immune cells, the roles of other metabolic pathways in B cell development remain unclear. Recently, the Fnip1/Folliculin/AMPK complex has emerged as a central mediator in maintaining metabolic homeostasis during B cell development (7, 8). Folliculin interacting protein-1 (Fnip1) is an evolutionarily conserved cytoplasmic protein originally discovered through its interaction with Folliculin (Flcn), a protein mutated in the rare autosomal dominant disorder Birt-Hogg-Dubé syndrome (BHDS)(9). Patients with BHDS develop benign hair follicle neoplasms, and are at high risk for developing lung cysts, pneumothorax, and renal tumors with a wide variety of histologies (reviewed in(10)). Fnip1 interacts in heteromultimeric complexes with Flcn, Fnip2, and AMPK, a master regulator of cellular metabolism (9). AMPK is phosphorylated during conditions of energy deprivation and responds by activating energy and nutrient producing processes such as mitochondrial biogenesis and autophagy, while simultaneously inhibiting energy and nutrient consuming pathways controlled by mTORC1. We previously generated *Fnip1*-deficient mice and showed that constitutive loss of *Fnip1* resulted in a complete block in B cell development at the pre-B cell stage, due in part to increased apoptosis (7, 8). Enforced expression of IgH and IgL chain proteins in *Fnip1*-null pre-B cells failed to rescue mature B cell development despite surface IgM expression, suggesting an intrinsic defect in cellular growth and differentiation pathways following disruption of *Fnip1*.

In this study we took a genetic approach to investigate molecular mechanisms of how Fnip1 controls B cell development. Our results reveal that Fnip1 coordinates multiple metabolic pathways regulated by AMPK, mTORC1, and Transcription Factor Binding to IgHM Enhancer 3 (TFE3) in order to maintain metabolic homeostasis necessary for pre-B cell survival and differentiation during metabolic stress.

Materials and Methods

Mice

Fnip1$^{-/-}$(7), *Bcl-x*$_L$^{Tg}, *Trp53*^{tm1Tyj}, *Raptor*$^{fl/fl}$, *Mb1-Cre*, *Tsc1*$^{fl/fl}$, *Prkaa1*$^{tm1.1Sjm}$, *Rag2*^{tm1Fwa}*Il2rg*^{tm1Wjl}, *Eμ-Myc*, and *EGFP-LC3* mice were described previously (11-19). *Bcl-x*$_L$^{Tg} mice were kindly provided by Tim Behrens, *Mb1-Cre* and *Eμ-Myc* mice were provided by Robert Eisenman, *Tsc1*$^{fl/fl}$ mice were provided by Raymond Yeung, and *EGFP-LC3* were provided by Mike Bevan, and ROSA26$^{lox\text{-}stop\text{-}lox\ tdTomato}$ mice were provided by R. Palmiter (20). *Trp53*^{tm1Tyj}, *Prkaa1*$^{tm1.1Sjm}$, mice were purchased from Jackson Labs, and *Rag2*^{tm1Fwa}*Il2rg*^{tm1Wjl} mice were purchased from Taconic Biosciences. Mice were maintained on a C57Bl/6J background or were backcrossed >10 generations, with the exception of *Tsc1*$^{fl/fl}$ and *Raptor*$^{fl/fl}$ crosses, which were on a mixed 129:C57Bl/6J background. Co-housed littermates of both sexes were used whenever possible. Animal studies were reviewed and approved by the University of Washington Institutional Animal Care and Use Committee.

Cell viability and proliferation assays

To assess apoptosis, cells were stained ex vivo with CellEvent Caspase 3/7 (Invitrogen, Carlsbad, CA) and Ghost dye live/dead viability stain (Tonbo Biosciences, San Diego, CA), and analyzed according to the manufacturers' instructions. Analysis of cellular proliferation in vivo was performed by i.p. BrdU injection (1 mg, BD Biosciences, San Jose, CA) ~16 hrs prior to harvest. Intracellular (IC) staining were performed according to the manufacturer with α–BrdU PerCP/Cy5.5 (BD Pharmingen, San Jose, CA).

Antibodies and flow cytometry

Cells were stained using Abs specific for mouse Ags: CD45R (B220) (various fluorochromes) (BD Pharmingen, BioLegend, San Diego, CA and Tonbo Biosciences); IgM (various fluorochromes, Jackson ImmuoResearch Laboratories, West Grove, PA); CD19 eFlour450, CD25 APC, MHC II APC (Tonbo Biosciences); CD43 PE, BP-1 PE, CD117 PE, CD24 (HSA) PE-Cy7, IgD FITC (BD Pharmingen); CD21 PerCP/Cy5.5 (BioLegend). IC staining was performed with IC fixation and permeabilization buffer (eBiosciences). Methanol fixation was performed for IC phospho (p)-S6R detection. Abs used for IC staining were p-ribosomal S6 protein (S6R) S235/236 PE (eBiosciences); p-AMPKα T172, c-Myc AF488 and p-Ulk1 S555 (Cell Signaling Technology, Danvers, MA). Donkey anti-rabbit Alexa-Fluor 647 (Life Technologies, Carlsbad CA) secondary Ab was used to detect unlabeled primary Abs. Data was collected using FACS Canto II or LSR II flow cytometers (BD Biosciences) and analyses were performed using FlowJo software (TreeStar, Ashland, OR).

Immunoblotting

Immunoblotting was performed on whole cell extracts from cultured immortalized MEFs derived from *Fnip1*$^{-/-}$ mouse embryos (21). Proteins were detected using Abs against LC3B (D11, Cell Signaling Technology, Danvers, MA) and GAPDH (loading control;D16H11, Cell Signaling Technology).

Cell labeling using NBD-PS

The phospholipid incorporation assay was performed with *Fnip1*$^{-/-}$ or *Fnip1*$^{+/-}$ BM using the fluorescent analog of phosphatidylserine, NBD-PS (Avanti Polar Lipids, Inc.). Briefly, cells were labeled with 5 μM NBD-PS in HBSS (Gibco)+5.5mM D-glucose, 20 mM HEPES at 15°C for 5 min. Labeling was quenched in HBSS+5.5 mM D-glucose, 20 mM HEPES, 1% lipid-free BSA for 5 min on ice followed by two washes in HBSS +5.5 mM D-glucose, 20 mM HEPES and staining with fluorescent antibodies for flow cytometric analysis.

Cell labeling using DQ-BSA

BM cells were stained with Abs for flow cytometry as above, stimulated for 1 hr with 10 ng/mL IL-7 in complete media, then labeled with 20 μg/ml DQ-BSA Green (Invitrogen) in complete media at 37 °C for 1 hour, followed by two washes with DPBS+3% FBS before flow cytometric analysis.

Imagestream® imaging flow cytometry

Cells were cultured ex vivo for 2-3 hrs or overnight and fixed as described above for detection of IC Ags using rat α–LAMP2 (Abcam), rabbit α–mTOR (Cell Signaling Technology), or rabbit α–TFE3 (Sigma) Abs. Donkey α-rabbit Alexa Fluor 647 and donkey α-rat Alexa Fluor 488 (Life Technologies) secondary Abs were used to detect primary Abs. Data were collected using an Imagestream® imaging flow cytometry X (Millipore) and analyses were performed with IDEAS software (Millipore).

Mass spectrometry-based proteomics

B cells were enriched from total BM from *Fnip1*$^{-/-}$ and *Fnip1*$^{+/+}$ littermates. Pre- and pro-B cells were enriched via positive selection with α-CD19 Ab-conjugated magnetic beads (EasySep, Stemcell Technologies) followed by FACS sorting for IgM negative cells, and were cultured overnight in rIL-7 (R&D systems). 2×10^6 cells from each replicate were then lysed using 8M Urea. Peptide enrichment and chromatography were performed as previously described. Following peptide quantification (Pierce quantitative fluorometric peptide assay), 1 ug of each sample was analyzed by mass spectrometry as described previously(22).

Statistical analyses

Statistical differences between two groups were analyzed by two-tailed unpaired Student's *t* tests with equal variance. Multiple group comparisons were made using one-way ANOVA with multiple comparisons post-hoc *t* tests. GraphPad Prism software (version 6; GraphPad Software, San Diego, CA) was used for analyses, and data were considered significant at *p≤0.05, **p≤0.001, ***p≤0.0001, ****p<0.00001. Center values shown on graphs represent means and error bars represent standard deviations. For all graphs, each point plotted represents the analysis of primary cells derived from a single mouse.

Results

Disruption of Fnip1 results in increased apoptosis of B cell progenitors.

To assess whether acute disruption of *Fnip1* affects B cell development in adult animals and not via deletion in embryonic/fetal/neonatal tissues, we crossed *Fnip1*$^{fl/fl}$ mice (8) with *Mx1-Cre* (21) mice, which express Cre recombinase from the IFN-responsive *Mx1* gene promoter. Cre expression is transiently induced in response to injection of the dsRNA analog polyinosinic:polycytidylic acid (poly I:C). We found that the percentage of immature and mature B cells (Hardy Fractions E and F, (23)) in the bone marrow (BM) were markedly reduced two wks following poly I:C injection (Fig.1A), while the representation of pro-B/early pre-B cells (Hardy Fractions A-C')) were slightly increased. This likely represents a developmental block, as Caspase 3/7^{+} apoptotic pro-B/pre-B cells increased 48 hrs after poly I:C administration (Supplemental Fig. 1A). To visualize *Fnip1*-deleted cells, *Fnip1*$^{fl/fl}$*Mx1*Cre mice were crossed with *tdTomato* Cre-reporter mice, which allows Cre-expressing cells to be identified via the expression of red fluorescent protein. A single injection of poly I:C resulted in ~90% tomato fluorescent protein (FP)$^{+}$ B220^{+}IgM^{-} proB/preB cells, ~80% tomatoFP^{+} B220^{lo}IgM^{+} immature B cells, and ~50% tomatoFP^{+} mature B220^{hi}IgM^{+} B cells by 48 hrs post-injection (Supplemental Fig. 1B). The reduction in tomatoFP+ cells during the pre-B to immature B cell stage is consistent with increased apoptosis and selection against the deleted allele with maturation. Although poly I:C-induced α/β IFN might synergize with *Fnip1*-deficiency to mediate cell death, both experimental and control mice were treated with poly I:C. These findings indicate that acute disruption of *Fnip1* leads to impaired development at the pre-B cell stage due in part to increased apoptosis.

Increased apoptosis of Fnip1-deficient B cell progenitors occurs independently of p53.

We next investigated the molecular mechanisms leading to increased apoptosis of *Fnip1*-deficient B cell progenitors. V(D)J recombination activates a p53-dependent checkpoint during B cell development, which induces apoptosis if recombination is prolonged or defective(24). Whereas *Fnip1*$^{-/-}$ pre-B cells express intracellular μ (ICμ) indicative of effective recombination, levels of ICmu are lower than in WT cells(7) possibly indicating a deficiency in survival during V(D)J recombination. We therefore asked whether increased apoptosis of *Fnip1*$^{-/-}$ B cell progenitors proceeds through a p53-dependent mechanism. *Fnip1*$^{-/-}$ mice were crossed with *p53*$^{-/-}$ mice to generate *Fnip1*$^{-/-}$*p53*$^{-/-}$ animals. p53 deficiency did not alter levels of apoptosis in *Fnip1*$^{-/-}$ B cell progenitors (Fig. 1B) and had no effect on B cell development (Supplementary Fig. 1C). These results suggest that the increase in pro-B/pre-B cell apoptosis following disruption of *Fnip1* occurs independently of p53.

Bcl-x_L overexpression restores cell viability but fails to rescue B cell development in Fnip1-deficient mice.

We next investigated whether overexpression of a pro-survival factor could restore normal B cell development. We crossed *Fnip1*$^{-/-}$ mice with transgenic (Tg) mice overexpressing *Bcl-x$_L$*, an anti-apoptotic member of the Bcl-2 family, in B cells (18). Although expression of the *Bcl-x$_L$* transgene markedly reduced apoptosis in *Fnip1*$^{-/-}$ pro- and pre-B cells (Fig. 1B),

Bcl-x_L only minimally (<10%) rescued the development of early and late pre-B (Fractions B, C/C' and D) and immature B cells (Fraction E) in the BM, and completely failed to restore the development of mature B cells in the BM (Fig. 1C,D) and spleen (not shown). An increase in Hardy Fractions B and C is reflective of *Bcl-x_L* Tg, which has been shown previously to increase the number of pro-B cells(18). Our results suggest that *Fnip1* deficiency results in impaired B cell development that is only partially dependent on cell survival, and that additional mechanisms contribute to blocked B cell differentiation.

Increased c-Myc-mediated cell growth and division fails to restore B cell development in Fnip1-deficient mice.

We previously found that constitutive loss of *Fnip1* resulted in enrichment for genes regulated by the Myc transcription factor ($p=1.8 \times 10^{-7}$) in microarray analysis of pre-B cells from *Fnip1*$^{-/-}$ compared to WT mice (7). c-Myc is important for pre-B cell development (21), and drives cell growth and proliferation while altering the apoptotic threshold of cells (reviewed in (25)). Analyses of c-Myc protein levels via IC staining revealed increased c-Myc in *Fnip1*$^{-/-}$ BM late pro-B cells (Fig. 2A, Supplemental Fig. 2D) indicating that decreased Myc levels were not responsible for blocked B cell development. Since increased c-Myc-driven metabolism might compensate for the absence of Fnip1, we tested whether B cell-specific overexpression of c-*Myc* could further stimulate B cell growth, metabolism, and drive maturation of *Fnip1*$^{-/-}$ pre-B cells by generating *Fnip1*$^{-/-}$ mice that overexpress c-Myc during B cell development (*Eμ-c-Myc*)(14). c-*Myc* overexpression failed to significantly increase proliferation of *Fnip1*$^{-/-}$ B cell progenitors (Fig. 2B), but efficiently increased cell growth, based on an increase in cell size (not shown). However, the c-Myc transgene only enabled development of a small population of pre-B and immature B cells in *Fnip1*$^{-/-}$ animals, and completely failed to rescue the development of circulating mature B cells in the BM (Fig. 2C) and periphery (not shown). These results indicate that stimulation of cellular growth, metabolism, and proliferation by overexpression of c-Myc is not sufficient to restore B cell development in the absence of Fnip1.

Disruption of Fnip1 increases AMPK activation, autophagy induction and flux.

Autophagy is a self-degradation process necessary to generate nutrients and energy during development and in response to energy stress. Because Fnip1 interacts with AMPK, a primary activator of autophagy, and mTORC1 inhibits autophagy (26), we examined whether *Fnip1* deficiency impacts autophagy during B cell development. Consistent with our previous report, we found *Fnip1*$^{-/-}$ pro- and pre-B cells exhibited increased AMPKα phosphorylation at Thr172, as well as increased phosphorylation of a direct substrate of AMPK, Unc-51 Like Autophagy Activating Kinase 1 (Ulk1 phospho-Ser555), which is thought to initiate autophagy (Fig. 3A, Supplemental Fig. 2D).

Initiation of autophagy may not lead to increased flux through the pathway if autophagosome/lysosome fusion is blocked. Therefore, we visualized autophagosomes by generating *Fnip1*$^{-/-}$ microtubule-associated protein 1A/1B-light chain 3-GFP (LC3-GFP) fusion mice. During autophagy, cytosolic LC3-I is conjugated to phosphatidylethanolamine (PE) to form LC3-II, which subsequently becomes incorporated into autophagosomes. *Fnip1*$^{-/-}$ pro- and pre-B cells displayed increased levels of LC3-GFP overall (LC3-I&-II),

which decreased in response to autophagy induction with rapamycin or amino acid (AA) restriction, but remained higher than *Fnip1*$^{+/-}$ cells (Fig. 3B). Imagestream® imaging flow cytometry revealed an increased number and size of LC3-GFP puncta (autophagosomes) in *Fnip1*$^{-/-}$ pro- and pre- B cells, which appeared largely unchanged during induction of autophagy with rapamycin, while puncta number decreased in control cells (Fig. 3B, lower panel). Since altered lysosome number or function can help differentiate between autophagy inhibition or maximally increased flux, we measured the number of lysosomes (number of IC spots of the lysosome marker LAMP2) using Imagestream® and examined lysosomal activity by evaluating IC fluorescence of proteolyzed DQ-BSA, which requires enzymatic cleavage to generate a fluorescent product. A higher percentage of *Fnip1*$^{-/-}$ pro- and pre-B cells had high numbers of lysosomes (Fig. 3C) as well as increased lysosomal activity during induction of autophagy with the Tat-D11 (Beclin 1) peptide compared to control cells (Supplementary Fig. S1D), which suggests increased autophagic flux. To investigate whether a defect in lipid turnover was responsible for increased autophagosome and lysosome numbers, we measured incorporation of the fluorescent phospholipid analog NBD-phosphatidylserine (NBD-PS) into *Fnip1*$^{-/-}$ pro- and pre-B cells. We found that incorporation of NBD-PS into IC membranes was increased in *Fnip1*$^{-/-}$ cells relative to *Fnip1*$^{+/-}$ controls (Fig. 3D), indicating lipid turnover is higher than usual in these cells. We next measured LC3-GFP co-localization with LAMP2 using Imagestream® to determine if disruption of Fnip1 results in defects in autophagosome-lysosome fusion, which could also result in increased organelle number and size. We found that autophagosome-lysosome co-localization was not different between *Fnip1*$^{-/-}$ and *Fnip1*$^{+/-}$ control cells, and both displayed increased co-localization following treatment with Bafilomycin A1, which blocks autophagy at the final step of the pathway by preventing digestion of autolysosomes (Fig. 3E).

To definitively assess the flux of autophagy in *Fnip1*$^{-/-}$ cells, we next performed IC staining of LC3-II in late pro-B cells after treatment with Bafilomycin A1 to block autophagy. Autophagic flux was then determined by comparing the ratio of LC3-II after Bafilomycin treatment to basal levels of LC3-II. Autophagy flux was increased in *Fnip1*$^{-/-}$ late pro-B cells relative to *Fnip1*$^{+/-}$ controls (Fig. 3F). We used immunoblotting to confirm this result, comparing LC3B-I and LC3B-II levels in response to Bafilomycin in *Fnip1*$^{+/-}$ and *Fnip1*$^{-/-}$ mouse embryonic fibroblasts (MEFs, Supplemental Fig. S1E). *Fnip1*$^{-/-}$ MEFs had a much higher basal ratio of membrane-bound:cytoplasmic LC3B (LC3B-II:LC3B-I, lower panel densitometry), and upon starvation converted LC3-I to LC3-II faster than control cells, confirming *Fnip1* deficiency increases autophagic flux. Together, these results indicate that disruption of *Fnip1* in B cell progenitors results in an increased number of autophagosomes and lysosomes, as well as increased autophagic flux compared to *Fnip1*$^{+/-}$ B cell progenitors.

mTORC1 signaling is aberrantly increased in Fnip1-deficient B cell progenitors

mTORC1 is activated by growth factors and sufficient AAs, which are transported to the lysosome resulting in activation of vacuolar ATPases (v-ATPases). Activated v-ATPases then stimulate guanine nucleotide exchange activity of the Ragulator complex towards the RagA/B/C/D GTPases, which recruit mTORC1 to the lysosome where mTOR is activated

(reviewed in(27)). While some studies have shown that constitutive *Fnip1* or *Flcn* deficiency in mice is associated with mTORC1 hyperactivation (7, 28-30), other investigations in cell lines have shown that Fnip1 and Folliculin positively regulate mTORC1 activity by functioning as Rag C/D GTPase activating proteins (GAPs) or Rag A/B guanine nucleotide exchange factors (GEFs) at the lysosomal surface, thus helping recruit and retain mTORC1 at the lysosome (31, 32). To further assess the roles of Fnip1 in mTORC1 activation during B cell development, we measured the size of BM B cell progenitors (indicative of cell growth) in $Fnip1^{-/-}$ and $Fnip1^{+/-}$ mice using flow cytometry. Cell size was increased in $Fnip1^{-/-}$ late pro-B cells relative to $Fnip1^{+/-}$ control pro-B cells, which correlates with the stage at which pre-B cells normally decrease in size during early B cell development (Fig. 4A). IC phosphorylated S6 ribosomal subunit (p-S6R), a substrate downstream of mTORC1, was increased in $Fnip1^{-/-}$ versus $Fnip1^{+/-}$ pro-B cells (Fig. 4B). Although mTORC1 activity decreases in $Fnip1^{-/-}$ pro-B cells in response to AA restriction, it remains inappropriately high relative to $Fnip1^{+/-}$ controls, both in the presence or absence of AAs (Fig. 4B). To address if Fnip1 modulates the pre-B cell proteome, we performed whole cell mass spectroscopy-based proteomics on sorted pro- and pre-B cells from $Fnip1^{-/-}$ and control littermates. Consistent with increased mTORC1 activity, we found multiple ribosomal proteins were more abundant in $Fnip1^{-/-}$ relative to $Fnip1^{+/-}$ control cells (Supplementary Table 1).

Since mTORC1 activity is regulated by recruitment to the lysosomal surface in response to AA sufficiency, we examined whether the increase in mTORC1 activation in $Fnip1^{-/-}$ pre-B cells was associated with altered localization at the lysosome. We assessed mTOR co-localization with lysosomes in $Fnip1^{-/-}$ versus $Fnip1^{+/-}$ B cell progenitors using IC staining for mTOR and LAMP2, followed by visualization with Imagestream® imaging flow cytometry. As expected, mTOR/lysosomal co-localization decreased in response to AA restriction in control cells (Fig. 4C left panel). However, $Fnip1^{-/-}$ cells exhibited much higher basal levels of mTOR/lysosomal co-localization, which decreased upon AA starvation but remained aberrantly high (Fig. 4C). We also observed increased co-localization of mTOR with lysosomes in MEFs derived from $Fnip1^{-/-}$ mice using fluorescence microscopy (Fig. 4D). Relative to $Fnip1^{+/-}$ control MEFs under nutrient-rich conditions, which should show the most co-localization, mTOR remained associated with lysosomes during AA deprivation in $Fnip1^{-/-}$ MEFs, indicating that Fnip1 is necessary for optimal inactivation of mTOR.

We next determined whether increased (inappropriate) localization of mTOR to the lysosome in $Fnip1^{-/-}$ mice might impact cell survival in response to deprivation of arginine or lysine, which have been shown to be important for activating mTOR (33). We observed decreased numbers of $B220^{+}$ lymphocytes in $Fnip1^{-/-}$ BM cultured for 24 hrs in the absence of lysine or arginine compared to control BM, which displayed no significant loss of B cells in response to AA deprivation (Fig. 4E). These results suggest that Fnip1 may help terminate mTORC1 activation and increase cell survival in part by enabling mTOR translocation from the lysosomal surface to the cytosol in response to AA deprivation.

In light of these findings, we wondered whether genetic inhibition of mTORC1 activation could restore B cell development in $Fnip1^{-/-}$ mice. $Fnip1^{-/-}$ mice were crossed with

Raptor$^{fl/fl}$*Mb1-Cre* mice (1), which disrupts mTORC1 activation during B cell development. Inhibition of mTORC1 did not restore B cell development in *Fnip1*- and *Raptor*- double deficient animals (*Fnip1*$^{-/-}$*Raptor*$^{fl/fl}$*Mb1Cre*$^{+}$ mice) (Supplementary Fig. 2A-C) or *Fnip1*$^{-/-}$*Raptor*$^{fl/+}$*Mb1Cre*$^{+}$ mice (data not shown), which express attenuated levels of Raptor. These results are consistent with our previous study showing that prolonged treatment of *Fnip1*$^{-/-}$ mice with the mTORC1 inhibitor rapamycin was also unable to rescue B cell development (7).

Increased mTORC1-mediated cell growth does not inhibit pre-B cell development and fails to restore B cell development in Fnip1-deficient mice.

Since mTORC1 activity is essential for pre-B cell development, we next addressed whether the high mTORC1 activity we observed in *Fnip1*$^{-/-}$ pre-B cells could be compensatory for *Fnip1* deficiency. Thus, we tested whether further increasing mTORC1 activation would restore B cell development in *Fnip1*$^{-/-}$ mice. We disrupted *Tsc1* (a negative regulator of mTORC1) by breeding B cell-specific *Tsc1* null mice (*Tsc1*$^{fl/fl}$*Mb1-Cre*) to *Fnip1*$^{-/-}$ mice to generate *Tsc1* and *Fnip1* double deficient mice. *Fnip1*$^{-/-}$*Tsc1*$^{fl/fl}$*Mb1-Cre* animals develop renal disease before 4 wks of age (29), so we transplanted total BM cells from *Fnip1*$^{-/-}$*Tsc1*$^{fl/fl}$*Mb1-Cre* animals into irradiated *Rag2*$^{-/-}$*Il2rg*$^{-/-}$ or CD45.1 mismatched recipients. In accordance with high levels of mTORC1 signaling, both cell size and IC levels of p-S6R protein were increased in *Tsc1*$^{fl/fl}$*Mb-1Cre* and *Fnip1*$^{-/-}$*Tsc1*$^{fl/fl}$*Mb-1Cre* animals relative to *Fnip1*$^{-/-}$ mice (Supplementary Fig. S3A and data not shown). However, *Tsc1* deficiency failed to rescue B cell development, although a modest increase in B220^{lo}CD25^{+} late pre-B cells, B220^{lo}CD43^{-}IgM^{-} pro-and pre-B cells was noted in the BM (Supplementary Fig. S3B). Unlike *Raptor* deficiency, B cell-specific *Tsc1* deficiency does not inhibit B cell development. This evidence combined with the observation that conditional deletion of *Ampkα1* in B cells (*Ampkα1*$^{fl/fl}$*Mb1-Cre*) does not rescue B cell development in *Fnip1*$^{-/-}$ mice (Supplementary Fig. S3C) indicate aberrant mTORC1 or AMPK activation alone are not responsible for the developmental block in *Fnip1*$^{-/-}$ B cell progenitors.

Fnip1 is necessary for TFE3 inactivation in pro-and pre- B cells.

Both mTORC1 and the Folliculin/Fnip1/Fnip2 complex have been implicated in inhibiting lysosomal biogenesis through phosphorylation and cytoplasmic retention of TFE3 (34-37), which is considered a master regulator of lysosome gene expression. Since mTORC1 activity and lysosomal biogenesis were both increased in *Fnip1*$^{-/-}$ B cell progenitors, we hypothesized that disruption of *Fnip1* leads to increased TFE3 nuclear localization. To investigate this hypothesis we utilized imaging flow cytometry to examine the IC localization of TFE3 in *Fnip1*$^{-/-}$ and *Fnip1*$^{+/-}$ B cell progenitors. TFE3 nuclear localization, based on co-localization of TFE3 and DAPI staining, increased in response to AA restriction in both control and *Fnip1*$^{-/-}$ pro/pre-B cells as expected (Fig. 5A). Notably, *Fnip1*$^{-/-}$ cells displayed significantly higher TFE3 nuclear localization than control cells both in the presence and absence of essential AAs (Fig. 5A), despite higher levels of lysosome-associated mTORC1 under the same conditions (Fig. 4C and 4D). Increased TFE3 nuclear localization also correlated with increased transcriptional activation of known TFE3 target genes including *Gpnmb*, *Pgc1a*, *Rragd*, and *Lamp1* (Fig. 5B)(7). These results collectively

suggest that in B cell progenitors, Fnip1 is required for retention of TFE3 in the cytosol under nutrient replete conditions, when mTORC1 is activated.

Discussion

Constitutive disruption of *Fnip1* in mice results in a complete absence of mature B cells and Abs due to a block in B cell development at the pre-B cell stage (7, 8) and decreased survival of B cell progenitors in response to metabolic stressors such as nutrient deprivation and pre-BCR crosslinking. In this study, we found that increased apoptosis occurred independently of p53, and that rescuing pre-B cell survival with a *Bcl*-x_L transgene failed to efficiently restore mature B cell development. These results suggest that Fnip1 regulates B cell development through mechanisms that are only partially dependent on pre-B cell survival. While our results differ from previously published results showing that Bcl-2 expression was able to rescue B cell development in *Fnip1*-deficient mice (8, 38), Bcl-2 and Bcl-$_{XL}$ are not completely functionally redundant; Bcl-x_L is more stable than Bcl-2 (39) and inhibits both Bax and Bak, direct effectors of mitochondrial apoptosis, while Bcl-2 does not do so. Bcl-$_{XL}$ and Bcl-2 have different effects on hematopoietic cell fate when ectopically expressed in multipotent progenitor cells; Bcl-x_L supports erythroid cell fate whereas Bcl-2 supports myeloid cell fates(40). Our studies suggest that the unique functions of Fnip1 in B cells include enabling efficient mTORC1 dissociation from the lysosome in response to AA deprivation, and limiting translocation of TFE3 to the nucleus. These results highlight multiple mechanisms whereby Fnip1 maintains metabolic homeostasis during B cell development.

Fnip1 was cloned based on physical interactions with Flcn and all three subunits of AMPK. AMPK phosphorylates both Fnip1 and Flcn, although the consequences of this modification remain unclear. In this study, we found that AMPK was activated in *Fnip1*-deficient pro-B/pre-B cells, which correlated with increased AMPK-mediated phosphorylation of ULK1 (a positive regulator of autophagy), increased induction of autophagy, and increased flux of autophagy relative to control cells. Elevated levels of autophagy in *Fnip1*$^{-/-}$ B cell progenitors did not increase further in response to AA deprivation, consistent with the notion that autophagy flux was near maximum. Previous studies have suggested that autophagy is also increased in flies lacking the Drosophila *Flcn* homologue *DBHD* (41), as well as in *C. elegans* and MEFs lacking *Flcn* (42). In addition, another group reported that basal autophagy was increased in *Fnip1*$^{-/-}$ B cell progenitors (38). These previous studies are consistent with our data showing increased autophagic flux in pro- and pre-B cells following disruption of *Fnip1*. However, Dunlop et al found that Flcn and Fnip1 positively regulate autophagy in human kidney cells via interaction with GABARAP, an autophagy component which is crucial for autophagosome formation and sequestration of cytosolic cargo into vesicles (42). Increased levels of SQSTM-1 and LC3 were observed in *Flcn*-deficient MEFs and renal tumor cells from a BHDS patient, but were interpreted as indicative of impaired autophagy, while autophagic flux was not examined. These studies highlight the complexity of the interactions between the Flcn/Fnip1/Fnip2 complex and autophagic pathways, suggesting that the impact of Flcn/Fnip deficiency on autophagic flux may be tissue dependent and/or influenced by the energetic state of the tissues examined.

Surprisingly, despite increased autophagy in *Fnip1*$^{-/-}$ B cell progenitors, we also found that mTORC1 activity and lysosomal localization were aberrantly increased, even under conditions of AMPK activation and AA restriction when mTORC1 should be cytosolic and inactive. These results suggest that at least in some cell types, Fnip1 may be necessary for AMPK to efficiently inactivate mTORC1, which is consistent with findings by others in human cell lines and MEFs. In particular, Nagashima *et al* found that ubiquitination and degradation of Fnip2 led to the dissociation of Flcn from the lysosome and constitutive association and activation of mTOR at the lysosomal surface regardless of nutrient status (43). Zhang *et al* demonstrated that the scaffold protein Axin tethers AMPK to the surface of endosomes and lysosomes where it is activated by the v-ATPase-Ragulator complex in response to glucose deprivation (44). These studies collectively suggest that the Fnip1/Fnip2/Flcn complex could serve as a molecular scaffold allowing AMPK to interact with the lysosomal v-ATPase at the surface of lysosomes, thus modulating the ability of AMPK to inactivate mTORC1 under nutrient poor conditions. With both catabolic and anabolic pathways active concurrently, our results suggest that a significant energy imbalance in *Fnip1*-deficient B cell progenitors precludes survival during cellular stresses such as AA restriction, since mTORC1-driven nutrient consumption remains inflexibly high.

Despite significant elevations in mTORC1 and AMPK activity following disruption of *Fnip1*, we also found that deletion of the AMPKα1 subunit, or attenuation of mTORC1 activity through disruption of *Raptor* or treatment with Rapamycin, were unable to rescue B cell development in *Fnip1*$^{-/-}$ mice. In addition, increasing mTORC1 activity through B cell specific disruption of *Tsc1* did not recapitulate the block in early development of *Fnip1*$^{-/-}$ B cells. These results indicate that additional factors may contribute to impaired B cell development in *Fnip1*$^{-/-}$ mice. Indeed, we found increased nuclear localization of the TFE3 transcription factor in *Fnip1*-deficient pro- and pre-B cells relative to control cells. Nuclear localization of TFE3 correlated with increased lysosome numbers and activity, mitochondrial biogenesis, expression of TFE3 target genes (7), and autophagy. Accordingly, previous studies showed that inactivation of *FLCN* in human renal cancer cell lines induced TFE3 transcriptional activity by increasing its nuclear localization (36), and that inactivation of FLCN in human fetal lung fibroblasts inhibited canonical WNT signaling, which could be completely restored only by silencing TFE3 (45). Other studies have similarly reported that the Flcn/Fnip1/Fnip2 complex is required for mouse ES cell (35), hematopoietic stem cell (46), and osteoclast (37) differentiation by restricting nuclear localization and activity of TFE3.

Previous studies have shown that mTORC1 inhibits TFE3 transcriptional activity by phosphorylating and inhibiting TFE3 nuclear translocation (35). The apparent paradox of high levels of mTORC1 activation concurrent with nuclear TFE3 in *Fnip1*-deficient pre-B cells was similarly seen by Wada *et al* in *Flcn*-deficient murine adipose tissue (34). In that study, mTORC1-mediated phosphorylation and cytoplasmic retention of TFE3 was dependent on Flcn, whereas phosphorylation of other downstream substrates such as S6K appeared independent of Flcn function. This may be explained by the findings that the Flcn/Fnip complex acts as a GAP converting RagC/D^{GTP} to RagC/D^{GDP}(31), and TFE3 is recruited to the lysosome by binding inactive RagC/D^{GDP} (47). Thus, despite increased mTORC1 activity and lysosomal localization in the absence of the Fnip1/Flcn complex,

TFE3 may not be recruited to the lysosome to be phosphorylated by mTORC1. The resulting aberrantly high levels of TFE3 transcriptional activity may contribute to impaired B cell development, as has been observed with HSC and osteoclast differentiation. The ability of mTORC1 to phosphorylate and inhibit nuclear localization of TFE3/Tfeb in a Flcn/Fnip1/Fnip2-dependent manner may be a conserved mechanism enabling nutrient sensing pathways to regulate differentiation of immune and other cell types.

Supplementary Material

Refer to Web version on PubMed Central for supplementary material.

Acknowledgements

The authors thank T. Chang for assistance with Imagestream® data collection and analysis, and R. Shaw for immortalization of *Fnip1*$^{-/-}$ MEFs. We thank L. Kang, J. Chan, and M. Torres for help with the mouse colony.

Support: This work was supported by NIH grants R21AI109020, R01AI092093, R56AI092093 (B.M.I.); K01OD010554 (J.A.R.); K01OD21421 (T.I). L.S.S. is funded in part with Federal funds from the Frederick National Laboratory for Cancer Research, NIH under contract HHSN261200800001E.

Abbreviations:

mTOR	mechanistic target of Rapamycin
mTORC1	mTOR complex 1
mTORC2	mTOR complex 2
Fnip1	Folliculin Interacting Protein-1
Flcn	Folliculin
AMPK	5’AMP-activated protein kinase
TSC1	tuberous sclerosis-1
4EBP1	eIF4E-binding protein 1
BM	bone marrow
IC	intracellular
poly I:C	polyinosinic-polycytidylic acid
LC3	Microtubule-associated protein 1A/1B-light chain

References

1. Iwata TN, Ramirez JA, Tsang M, Park H, Margineantu DH, Hockenbery DM, and Iritani BM. 2016 Conditional Disruption of Raptor Reveals an Essential Role for mTORC1 in B Cell Development, Survival, and Metabolism. J Immunol 197: 2250–2260. [PubMed: 27521345]
2. Ramadani F, Bolland DJ, Garcon F, Emery JL, Vanhaesebroeck B, Corcoran AE, and Okkenhaug K. 2010 The PI3K isoforms p110alpha and p110delta are essential for pre-B cell receptor signaling and B cell development. Sci Signal 3: ra60. [PubMed: 20699475]

3. Baracho GV, Cato MH, Zhu Z, Jaren OR, Hobeika E, Reth M, and Rickert RC. 2014 PDK1 regulates B cell differentiation and homeostasis. Proc Natl Acad Sci U S A 111: 9573–9578. [PubMed: 24979759]

4. Yu M, Chen Y, Zeng H, Zheng Y, Fu G, Zhu W, Broeckel U, Aggarwal P, Turner A, Neale G, Guy C, Zhu N, Chi H, Wen R, and Wang D. 2017 PLCgamma-dependent mTOR signalling controls IL-7-mediated early B cell development. Nat Commun 8: 1457. [PubMed: 29133930]

5. Zeng H, Yu M, Tan H, Li Y, Su W, Shi H, Dhungana Y, Guy C, Neale G, Cloer C, Peng J, Wang D, and Chi H. 2018 Discrete roles and bifurcation of PTEN signaling and mTORC1-mediated anabolic metabolism underlie IL-7-driven B lymphopoiesis. Sci Adv 4: eaar5701. [PubMed: 29399633]

6. Iwata TN, Ramirez-Komo JA, Park H, and Iritani BM. 2017 Control of B lymphocyte development and functions by the mTOR signaling pathways. Cytokine Growth Factor Rev 35: 47–62. [PubMed: 28583723]

7. Park H, Staehling K, Tsang M, Appleby MW, Brunkow ME, Margineantu D, Hockenbery DM, Habib T, Liggitt HD, Carlson G, and Iritani BM. 2012 Disruption of Fnip1 Reveals a Metabolic Checkpoint Controlling B Lymphocyte Development. Immunity.

8. Baba M, Keller JR, Sun HW, Resch W, Kuchen S, Suh HC, Hasumi H, Hasumi Y, Kieffer-Kwon KR, Gonzalez CG, Hughes RM, Klein ME, Oh HF, Bible P, Southon E, Tessarollo L, Schmidt LS, Linehan WM, and Casellas R. 2012 The folliculin-FNIP1 pathway deleted in human Birt-Hogg-Dube syndrome is required for murine B-cell development. Blood 120: 1254–1261. [PubMed: 22709692]

9. Baba M, Hong SB, Sharma N, Warren MB, Nickerson ML, Iwamatsu A, Esposito D, Gillette WK, Hopkins RF 3rd, Hartley JL, Furihata M, Oishi S, Zhen W, Burke TR Jr., Linehan WM, Schmidt LS, and Zbar B. 2006 Folliculin encoded by the BHD gene interacts with a binding protein, FNIP1, and AMPK, and is involved in AMPK and mTOR signaling. Proc Natl Acad Sci U S A 103: 15552–15557. [PubMed: 17028174]

10. Schmidt LS, and Linehan WM. 2015 Clinical Features, Genetics and Potential Therapeutic Approaches for Birt-Hogg-Dube Syndrome. Expert Opin Orphan Drugs 3: 15–29. [PubMed: 26581862]

11. Polak P, Cybulski N, Feige JN, Auwerx J, Ruegg MA, and Hall MN. 2008 Adipose-specific knockout of raptor results in lean mice with enhanced mitochondrial respiration. Cell Metab 8: 399–410. [PubMed: 19046571]

12. Jacks T, Remington L, Williams BO, Schmitt EM, Halachmi S, Bronson RT, and Weinberg RA. 1994 Tumor spectrum analysis in p53-mutant mice. Curr Biol 4: 1–7. [PubMed: 7922305]

13. Hobeika E, Thiemann S, Storch B, Jumaa H, Nielsen PJ, Pelanda R, and Reth M. 2006 Testing gene function early in the B cell lineage in mb1-cre mice. Proc Natl Acad Sci U S A 103: 13789–13794. [PubMed: 16940357]

14. Adams JM, Harris AW, Pinkert CA, Corcoran LM, Alexander WS, Cory S, Palmiter RD, and Brinster RL. 1985 The c-myc oncogene driven by immunoglobulin enhancers induces lymphoid malignancy in transgenic mice. Nature 318: 533–538. [PubMed: 3906410]

15. Meikle L, McMullen JR, Sherwood MC, Lader AS, Walker V, Chan JA, and Kwiatkowski DJ. 2005 A mouse model of cardiac rhabdomyoma generated by loss of Tsc1 in ventricular myocytes. Hum Mol Genet 14: 429–435. [PubMed: 15601645]

16. Nakada D, Saunders TL, and Morrison SJ. 2010 Lkb1 regulates cell cycle and energy metabolism in haematopoietic stem cells. Nature 468: 653–658. [PubMed: 21124450]

17. Mizushima N, Yamamoto A, Matsui M, Yoshimori T, and Ohsumi Y. 2004 In vivo analysis of autophagy in response to nutrient starvation using transgenic mice expressing a fluorescent autophagosome marker. Mol Biol Cell 15: 1101–1111. [PubMed: 14699058]

18. Fang W, Mueller DL, Pennell CA, Rivard JJ, Li YS, Hardy RR, Schlissel MS, and Behrens TW. 1996 Frequent aberrant immunoglobulin gene rearrangements in pro-B cells revealed by a bcl-xL transgene. Immunity 4: 291–299. [PubMed: 8624819]

19. Kuhn R, Schwenk F, Aguet M, and Rajewsky K. 1995 Inducible gene targeting in mice. Science 269: 1427–1429. [PubMed: 7660125]

20. Madisen L, Zwingman TA, Sunkin SM, Oh SW, Zariwala HA, Gu H, Ng LL, Palmiter RD, Hawrylycz MJ, Jones AR, Lein ES, and Zeng H. 2010 A robust and high-throughput Cre reporting

and characterization system for the whole mouse brain. Nat Neurosci 13: 133–140. [PubMed: 20023653]

21. Habib T, Park H, Tsang M, de Alboran IM, Nicks A, Wilson L, Knoepfler PS, Andrews S, Rawlings DJ, Eisenman RN, and Iritani BM. 2007 Myc stimulates B lymphocyte differentiation and amplifies calcium signaling. J Cell Biol 179: 717–731. [PubMed: 17998397]
22. Tampella G, Kerns HM, Niu D, Singh S, Khim S, Bosch KA, Garrett ME, Moguche A, Evans E, Browning B, Jahan TA, Nacht M, Wolf-Yadlin A, Plebani A, Hamerman JA, Rawlings DJ, and James RG. 2015 The Tec Kinase-Regulated Phosphoproteome Reveals a Mechanism for the Regulation of Inhibitory Signals in Murine Macrophages. J Immunol 195: 246–256. [PubMed: 26026062]
23. Hardy RR, Carmack CE, Shinton SA, Kemp JD, and Hayakawa K. 1991 Resolution and characterization of pro-B and pre-pro-B cell stages in normal mouse bone marrow. J Exp Med 173: 1213–1225. [PubMed: 1827140]
24. Guidos CJ, Williams CJ, Grandal I, Knowles G, Huang MT, and Danska JS. 1996 V(D)J recombination activates a p53-dependent DNA damage checkpoint in scid lymphocyte precursors. Genes Dev 10: 2038–2054. [PubMed: 8769647]
25. McMahon SB 2014 MYC and the control of apoptosis. Cold Spring Harb Perspect Med 4: a014407. [PubMed: 24985130]
26. Kim J, Kundu M, Viollet B, and Guan KL. 2011 AMPK and mTOR regulate autophagy through direct phosphorylation of Ulk1. Nat Cell Biol 13: 132–141. [PubMed: 21258367]
27. Saxton RA, and Sabatini DM. 2017 mTOR Signaling in Growth, Metabolism, and Disease. Cell 169: 361–371.
28. Reyes NL, Banks GB, Tsang M, Margineantu D, Gu H, Djukovic D, Chan J, Torres M, Liggitt HD, Hirenallur SD, Hockenbery DM, Raftery D, and Iritani BM. 2015 Fnip1 regulates skeletal muscle fiber type specification, fatigue resistance, and susceptibility to muscular dystrophy. Proc Natl Acad Sci U S A 112: 424–429. [PubMed: 25548157]
29. Centini R, Tsang M, Iwata T, Park H, Delrow J, Margineantu D, Iritani BM, Gu H, Liggitt HD, Kang J, Kang L, Hockenbery DM, Raftery D, and Iritani BM. 2018 Loss of Fnip1 alters kidney developmental transcriptional program and synergizes with TSC1 loss to promote mTORC1 activation and renal cyst formation. PLoS One 13: e0197973. [PubMed: 29897930]
30. Hasumi Y, Baba M, Hasumi H, Huang Y, Lang M, Reindorf R, Oh HB, Sciarretta S, Nagashima K, Haines DC, Schneider MD, Adelstein RS, Schmidt LS, Sadoshima J, and Marston Linehan W. 2014 Folliculin (Flcn) inactivation leads to murine cardiac hypertrophy through mTORC1 deregulation. Hum Mol Genet 23: 5706–5719. [PubMed: 24908670]
31. Tsun ZY, Bar-Peled L, Chantranupong L, Zoncu R, Wang T, Kim C, Spooner E, and Sabatini DM. 2013 The folliculin tumor suppressor is a GAP for the RagC/D GTPases that signal amino acid levels to mTORC1. Mol Cell 52: 495–505. [PubMed: 24095279]
32. Petit CS, Roczniak-Ferguson A, and Ferguson SM. 2013 Recruitment of folliculin to lysosomes supports the amino acid-dependent activation of Rag GTPases. J Cell Biol 202: 1107–1122. [PubMed: 24081491]
33. Bar-Peled L, Chantranupong L, Cherniack AD, Chen WW, Ottina KA, Grabiner BC, Spear ED, Carter SL, Meyerson M, and Sabatini DM. 2013 A Tumor suppressor complex with GAP activity for the Rag GTPases that signal amino acid sufficiency to mTORC1. Science 340: 1100–1106. [PubMed: 23723238]
34. Wada S, Neinast M, Jang C, Ibrahim YH, Lee G, Babu A, Li J, Hoshino A, Rowe GC, Rhee J, Martina JA, Puertollano R, Blenis J, Morley M, Baur JA, Seale P, and Arany Z. 2016 The tumor suppressor FLCN mediates an alternate mTOR pathway to regulate browning of adipose tissue. Genes Dev 30: 2551–2564. [PubMed: 27913603]
35. Betschinger J, Nichols J, Dietmann S, Corrin PD, Paddison PJ, and Smith A. 2013 Exit from pluripotency is gated by intracellular redistribution of the bHLH transcription factor TFE3. Cell 153: 335–347. [PubMed: 23582324]
36. Hong SB, Oh H, Valera VA, Baba M, Schmidt LS, and Linehan WM. 2010 Inactivation of the FLCN tumor suppressor gene induces TFE3 transcriptional activity by increasing its nuclear localization. PLoS One 5: e15793. [PubMed: 21209915]

37. Baba M, Endoh M, Ma W, Toyama H, Hirayama A, Nishikawa K, Takubo K, Hano H, Hasumi H, Umemoto T, Hashimoto M, Irie N, Esumi C, Kataoka M, Nakagata N, Soga T, Yao M, Kamba T, Minami T, Ishii M, and Suda T. 2018 Folliculin Regulates Osteoclastogenesis Through Metabolic Regulation. J Bone Miner Res 33: 1785–1798. [PubMed: 29893999]

38. Siggs OM, Stockenhuber A, Deobagkar-Lele M, Bull KR, Crockford TL, Kingston BL, Crawford G, Anzilotti C, Steeples V, Ghaffari S, Czibik G, Bellahcene M, Watkins H, Ashrafian H, Davies B, Woods A, Carling D, Yavari A, Beutler B, and Cornall RJ. 2016 Mutation of Fnip1 is associated with B-cell deficiency, cardiomyopathy, and elevated AMPK activity. Proc Natl Acad Sci U S A 113: E3706–3715. [PubMed: 27303042]

39. Chen HC, Kanai M, Inoue-Yamauchi A, Tu HC, Huang Y, Ren D, Kim H, Takeda S, Reyna DE, Chan PM, Ganesan YT, Liao CP, Gavathiotis E, Hsieh JJ, and Cheng EH. 2015 An interconnected hierarchical model of cell death regulation by the BCL-2 family. Nat Cell Biol 17: 1270–1281. [PubMed: 26344567]

40. Haughn L, Hawley RG, Morrison DK, von Boehmer H, and Hockenbery DM. 2003 BCL-2 and BCL-XL restrict lineage choice during hematopoietic differentiation. J Biol Chem 278: 25158–25165. [PubMed: 12721288]

41. Liu W, Chen Z, Ma Y, Wu X, Jin Y, and Hou S. 2013 Genetic characterization of the Drosophila birt-hogg-dube syndrome gene. PLoS One 8: e65869. [PubMed: 23799055]

42. Dunlop EA, Seifan S, Claessens T, Behrends C, Kamps MA, Rozycka E, Kemp AJ, Nookala RK, Blenis J, Coull BJ, Murray JT, van Steensel MA, Wilkinson S, and Tee AR. 2014 FLCN, a novel autophagy component, interacts with GABARAP and is regulated by ULK1 phosphorylation. Autophagy 10: 1749–1760. [PubMed: 25126726]

43. Nagashima K, Fukushima H, Shimizu K, Yamada A, Hidaka M, Hasumi H, Ikebe T, Fukumoto S, Okabe K, and Inuzuka H. 2017 Nutrient-induced FNIP degradation by SCFbeta-TRCP regulates FLCN complex localization and promotes renal cancer progression. Oncotarget 8: 9947–9960. [PubMed: 28039480]

44. Zhang CS, Jiang B, Li M, Zhu M, Peng Y, Zhang YL, Wu YQ, Li TY, Liang Y, Lu Z, Lian G, Liu Q, Guo H, Yin Z, Ye Z, Han J, Wu JW, Yin H, Lin SY, and Lin SC. 2014 The lysosomal v-ATPase-Ragulator complex is a common activator for AMPK and mTORC1, acting as a switch between catabolism and anabolism. Cell Metab 20: 526–540. [PubMed: 25002183]

45. Kennedy JC, Khabibullin D, Hougard T, Nijmeh J, Shi W, and Henske EP. 2019 Loss of FLCN inhibits canonical WNT signaling via TFE3. Hum Mol Genet.

46. Baba M, Toyama H, Sun L, Takubo K, Suh HC, Hasumi H, Nakamura-Ishizu A, Hasumi Y, Klarmann KD, Nakagata N, Schmidt LS, Linehan WM, Suda T, and Keller JR. 2016 Loss of Folliculin Disrupts Hematopoietic Stem Cell Quiescence and Homeostasis Resulting in Bone Marrow Failure. Stem Cells 34: 1068–1082. [PubMed: 27095138]

47. Villegas F, Lehalle D, Mayer D, Rittirsch M, Stadler MB, Zinner M, Olivieri D, Vabres P, Duplomb-Jego L, De Bont E, Duffourd Y, Duijkers F, Avila M, Genevieve D, Houcinat N, Jouan T, Kuentz P, Lichtenbelt KD, Thauvin-Robinet C, St-Onge J, Thevenon J, van Gassen KLI, van Haelst M, van Koningsbruggen S, Hess D, Smallwood SA, Riviere JB, Faivre L, and Betschinger J. 2019 Lysosomal Signaling Licenses Embryonic Stem Cell Differentiation via Inactivation of TFE3. Cell Stem Cell 24: 257–270 e258. [PubMed: 30595499]

Key points:

- Fnip1 is required for pre-B cell development/survival independent of p53 and Bcl_{XL}
- Fnip1 is required for optimal inhibition of mTORC1 in response to aa restriction
- Fnip1 regulates TFE3 nuclear translocation and lysosome biogenesis in pre-B cells

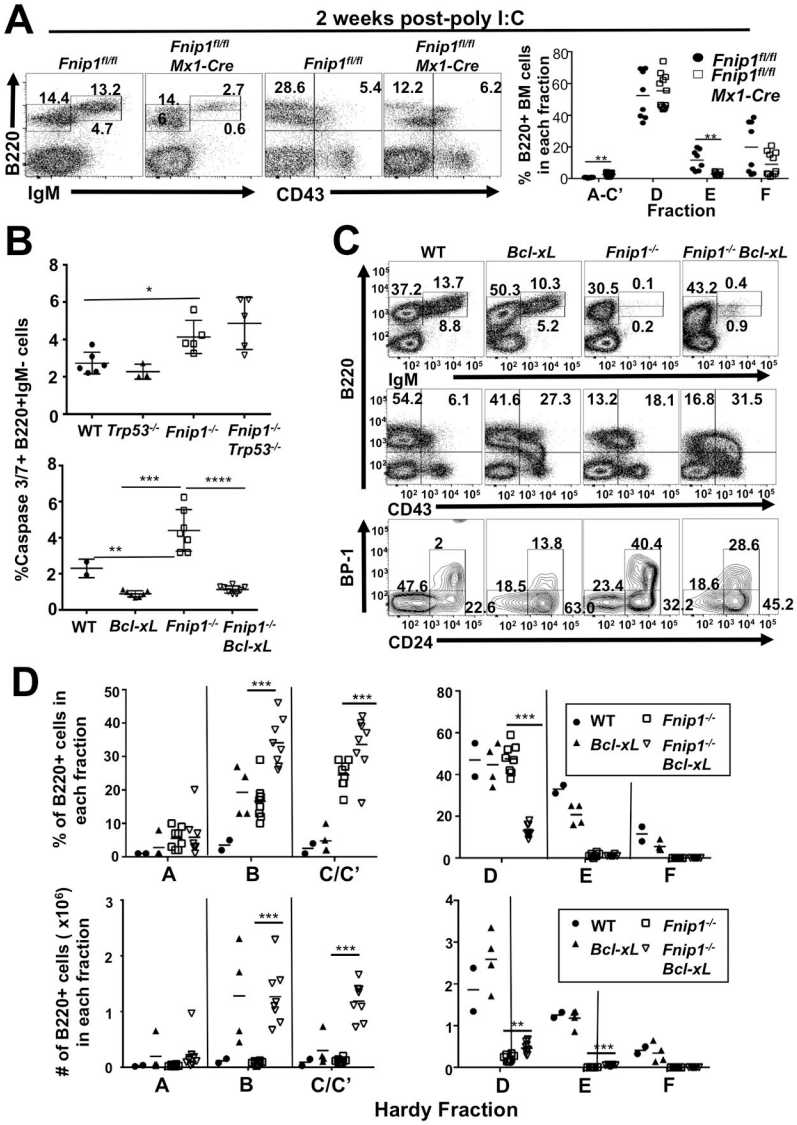

FIGURE 1.

Disruption of Fnip1 results in increased apoptosis. (**A**) Representative flow cytometric analyses of bone marrow (BM) cells from *Fnip1*$^{fl/fl}$ or *Fnip1*$^{fl/fl}$*Mx1-Cre* mice 13 days after deletion of *Fnip1* via poly I:C (pI:C) injection. Shown are gated lymphocytes (FSC/SSC) following staining for B220 (CD45R), IgM and CD43 (Ly48). Numbers on the plots represent the frequencies of the gated populations. The scatter plot (right panel) shows frequencies of B220^{+} BM cells in various developmental fractions (Hardy fractions). **=p<0.005 *t*-test (**B**) *p53* deletion and *Bcl-x*$_L$ overexpression fail to rescue B cell development in *Fnip1*-deficient mice. Scatter plots show frequencies of cleaved Caspase 3/7 substrate in B220^{+}IgM^{-} BM cells from wildtype (WT), *Fnip1*$^{-/-}$, *Trp53*$^{-/-}$ and *Fnip1*$^{-/-}$*Trp53*$^{-/-}$ mice (upper panel), or *Bcl-x*$_L$ and *Fnip1*$^{-/-}$*Bcl-x*$_L$ mice (lower panel). p≤0.0001 one-way ANOVA (**C**) Representative flow cytometric analyses of BM cells from WT, *Fnip1*$^{-/-}$, *Bcl-x*$_L$ and *Fnip1*$^{-/-}$*Bcl-x*$_L$ mice are shown gated on lymphocytes and stained for B220, IgM, CD43, BP-1 (Ly-51, CD249) and CD24 (HSA). **(D)** Scatter plots show

developmental (Hardy) fractions representing frequency (bottom left panel) and absolute number (bottom right panel) of cells from these mice. Gating for fractions: A=$B220^{+}CD43^{+}CD24^{-}BP\text{-}1^{-}$, B=$B220^{+}CD43^{+}CD24^{+}BP\text{-}1^{-}$, C/C'=$B220^{+}CD43^{+}CD24^{+}BP\text{-}1^{+}$, D=$B220^{lo}CD43^{-}IgM^{-}$, E=$B220^{lo}CD43^{-}IgM^{+}$, F=$B220^{hi}CD43^{-}IgM^{+}$.

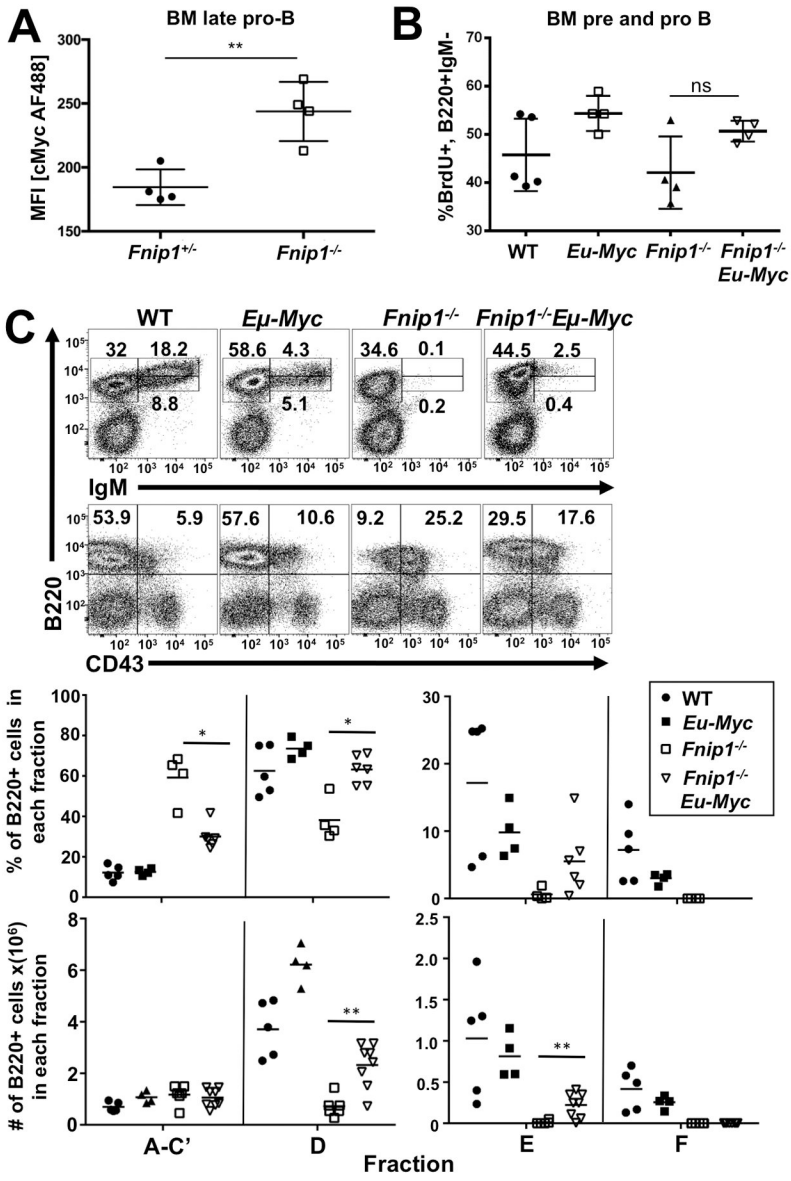

FIGURE 2.

Increased c-Myc-mediated cell growth fails to restore B cell development in *Fnip1*-deficient mice. Bar graphs show (**A**) mean fluorescence intensity (MFI) of IC c-Myc staining in $B220^{+}BP\text{-}1^{+}CD25^{-}$ late pro-B cells from *Fnip1*$^{+/-}$ or *Fnip1*$^{-/-}$ BM and (**B**) frequencies of $BrdU^{+}$ BM pro- and pre-B cells ($B220^{+}IgM^{-}$), which represent dividing cells from WT, *Eμ-Myc*, *Fnip1*$^{-/-}$, and *Eμ-Myc Fnip1*$^{-/-}$ mice. (**C**) Representative flow cytometric analyses of BM cells from WT, *Eμ-Myc*, *Fnip1*$^{-/-}$, and *Eμ-Myc Fnip1*$^{-/-}$ mice are shown gated on lymphocytes and stained for B220, IgM and CD43. **(D)** Scatter plots show developmental (Hardy) fractions representing frequency (top panel) and absolute number (bottom panel) of cells from these mice. Fraction A-C' is gated $B220^{+}CD43^{+}$.

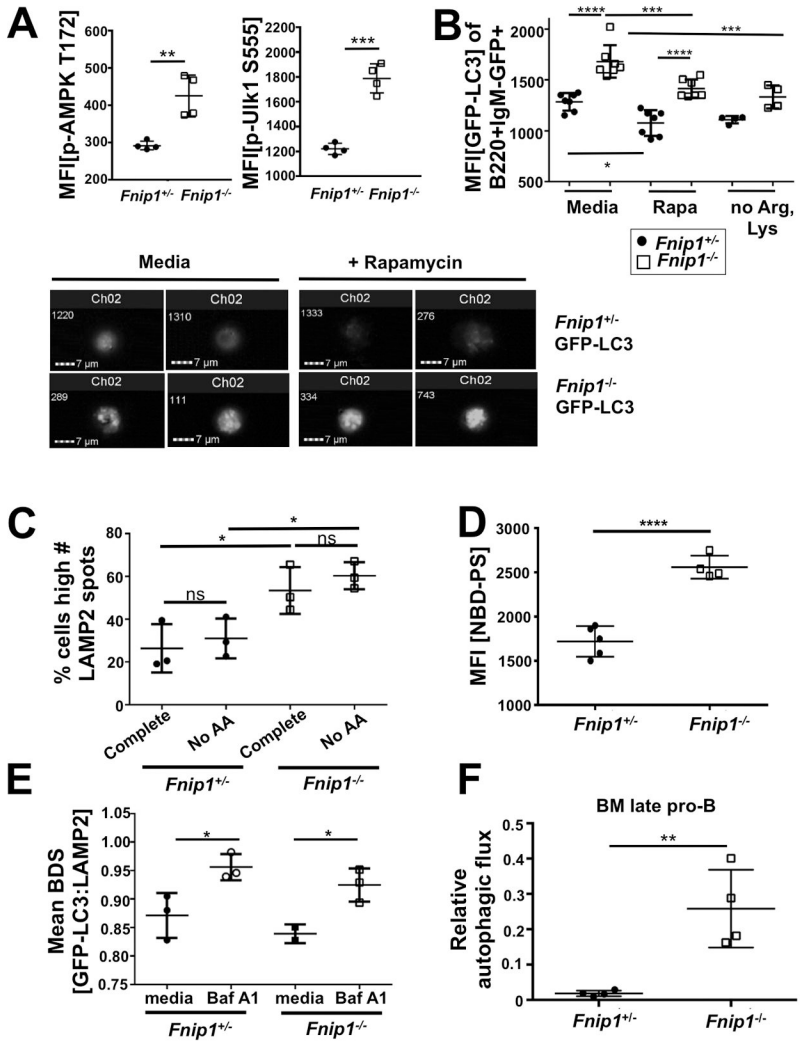

FIGURE 3.

Disruption of *Fnip1* increases autophagy induction and flux. Bar graphs show MFIs of (**A**) IC p-AMPK T172 staining (left panel) and IC p-Ulk1 S555 (right panel) on live-gated $B220^{+}IgM^{-}$ cells. (**B**) MFIs of EGFP-LC3 and representative images (imaging cytometry) of $B220^{+}IgM^{-}GFP^{+}$ BM cells from *EGFP-LC3 Fnip1*$^{+/-}$ or *EGFP-LC3 Fnip1*$^{-/-}$ mice without or with Rapamycin or arginine and lysine-free media for 24 hrs as measured by flow cytometry. $p<0.0001$ one-way ANOVA. (**C**) Frequency of $B220^{+}IgM^{-}$ BM cells from *Fnip1*$^{+/-}$ or *Fnip1*$^{-/-}$ mice with a high number of LAMP2 (lysosomal marker) spots, as measured by Imagestream® imaging flow cytometry, without or with 2 hrs of incubation in media without AAs. $p<0.0001$ one-way ANOVA. (**D**) MFI of $B220^{+}IgM^{-}$ BM cells from *Fnip1*$^{+/-}$ or *Fnip1*$^{-/-}$ mice incubated with fluorescent phospholipid analog NBD-phosphatidylserine for one minute. (**E**) Mean bright detail similarity (BDS) of GFP-LC3 and DyLight 650 LAMP2 from $B220^{+}IgM^{-}GFP^{+}$ BM cells from *EGFP-LC3 Fnip1*$^{+/-}$ or *EGFP-LC3 Fnip1*$^{-/-}$ mice cultured 24 hrs ex vivo in complete media or media without AAs supplemented with 10 nM Bafilomycin A1 (Baf A1) (blocks autophagy through inhibition of lysosomal degradation), as measured by imaging cytometry. Mean BDS is a measure of

colocalization. (**F**) Relative autophagic flux as measured by IC flow cytometric staining of LC3-II (autophagosome-bound LC3) in $B220^{+}IgM^{-}$ BM cells from *Fnip1*$^{+/-}$ or *Fnip1*$^{-/-}$ mice. The ratio of LC3-II after 2 hrs 100 nM Baf A1 treatment compared to basal levels of LC3-II is shown.

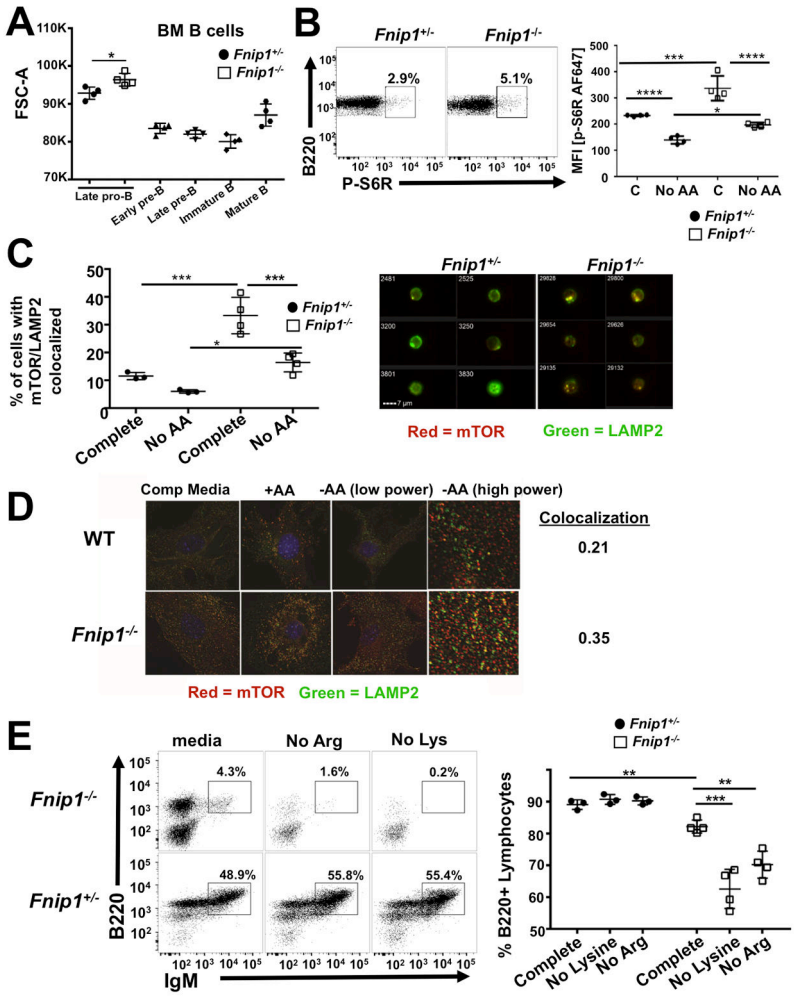

FIGURE 4.

mTORC1 signaling is aberrantly increased in *Fnip1*-deficient B cell progenitors. (**A**) Forward scatter (FSC-A, a measure of cell size) of BM B cells as measured by flow cytometry. Summary data from $Fnip1^{+/-}$ or $Fnip1^{-/-}$ mice. Late pro-B: $B220^{+}BP\text{-}1^{+}CD25^{-}$, early pre-B: $B220^{+}BP\text{-}1^{+}CD25^{+}$, late pre-B: $B220^{+}BP\text{-}1^{-}CD25^{+}$, immature B: $B220^{lo}IgM^{+}$, mature B: $B220^{hi}IgM^{+}$. (**B**) Representative dot plots (left panel) or summary MFI flow cytometry data without and with incubation in AA free media (right panel) of IC phospho-S6 ribosomal (P-S6R) staining (mTORC1 downstream substrate) from $B220^{+}IgM^{-}$ BM of $Fnip1^{+/-}$ or $Fnip1^{-/-}$ mice. $p<0.0001$ one-way ANOVA (**C**) Frequency of cells with colocalization (left panel) or representative images (right panels) of mTOR (red) and LAMP2 (green) IC staining in $Fnip1^{+/-}$ or $Fnip1^{-/-}$ BM gated $B220^{+}IgM^{-}$, as measured by imaging flow cytometry, without (left) or with (right) overnight incubation in AA free media. $p<0.0001$ one-way ANOVA. (**D**) Representative immunofluorescent images from $Fnip1^{+/-}$ or $Fnip1^{-/-}$ MEFs stained with anti-mTOR (red) and anti-LAMP2 (green) Abs. Cells were cultured ex vivo in AA-free media for 50 min +/− refeeding with AAs (1X concentration) for 10 min. Pearson's coefficient representing colocalization is shown (0=random distribution, 1=100% colocalization). (**E**) Representative dot plots of $B220^{+}IgM$

$^{+}$ cells (left panels) and frequency of B220^{+} lymphocytes (right panel) in *Fnip1*$^{+/-}$ or *Fnip1*$^{-/-}$ BM after 4 day ex vivo culture in complete media, media without lysine, or media without arginine.

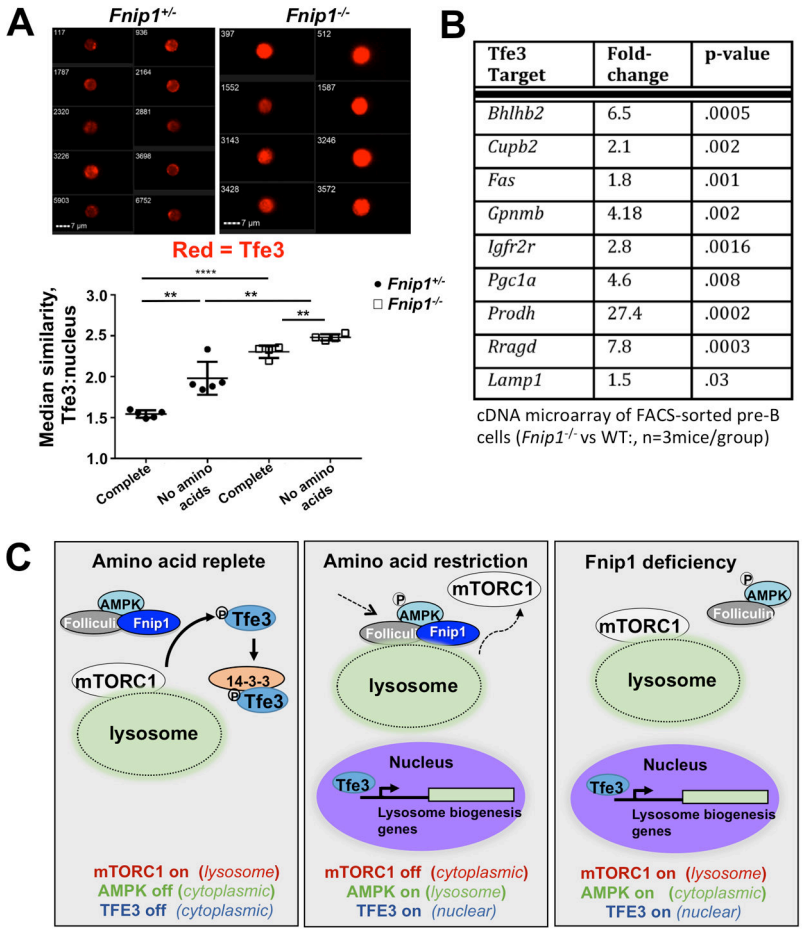

Tfe3 Target	Fold-change	p-value
Bhlhb2	6.5	.0005
Cupb2	2.1	.002
Fas	1.8	.001
Gpnmb	4.18	.002
Igfr2r	2.8	.0016
Pgc1a	4.6	.008
Prodh	27.4	.0002
Rragd	7.8	.0003
Lamp1	1.5	.03

FIGURE 5.

Fnip1 regulates TFE3 nuclear localization in B cell progenitors. (**A**) Median similarity (a measure of image overlap, lower panel) of TFE3 IC staining and nuclear staining (DAPI), and representative images (upper panels) of $B220^{+}IgM^{-}$ cells in *Fnip1*$^{+/-}$ or *Fnip1*$^{-/-}$ BM as measured by imaging flow cytometry. p<0.0001 one-way ANOVA. (**B**) Expression of selected TFE3 target genes as measured using Illumina cDNA microarray of FACs-sorted $B220^{+}IgM^{-}$ pro- and pre-B cells, *Fnip1*$^{-/-}$ vs. WT, n=3 mice/group. (**C**) Schematic model of signaling inside *Fnip1*-deficient B cells compared to normal B cells under nutrient replete or AA restricted conditions, showing dysregulation of mTORC1 and TFE3 localization in the absence of Fnip1.